A Method of Substrate Shaping to Improve Gain of Active-Element Pattern for Small Arrays

Taekki Lee, Dae-Heon Lee, Hosung Choo, and Gangil Byun

***Abstract*—This letter proposes a method of substrate subtraction to improve the gain of an active-element pattern for individual elements in a small array. The proposed method is applied to a three-element controlled reception pattern antenna array, whose radiating elements are printed on a high-dielectric ceramic substrate. Then, three identical fan-shaped areas, placed between the array elements, are subtracted from the substrate, and their shapes are adjusted to avoid unnecessary power losses caused by the fringing field effect, leakage fields, and surface currents. The effects of the subtracted areas are also investigated as parametric studies to demonstrate the effectiveness of the proposed substrate shaping method. The results show that the gain can be increased by 0.7 dB due to lower effective dielectric loss compared to the full substrate.**

***Index Terms*—Antenna substrate, controlled reception pattern antenna (CRPA) array, GPS array, phased array.**

I. Introduction

CIRCULAR arrays have been widely adopted for controlled reception pattern antenna (CRPA) applications due to their wide angular coverage of beam steering in both azimuth and elevation [1]−[4]. However, the beam steering capability is easily degraded when the aperture size of the array is restricted to a few centimeters in diameter. The conventional approach to this performance degradation is focused on modifying the shape of radiators using slot insertion as introduced in [5], fractal structures as in [6], and shape transformation as in [7]. Another approach to this problem is the use of high-dielectric substrates to further reduce the size for improved gain with lower mutual coupling strength between array elements [8]. In this approach, the antenna characteristics are easily affected by the fringing field effect, leakage fields confined between array elements, and surface currents induced on the ground platform. Thus, the shape of the substrates should be carefully considered as an important design parameter to improve the antenna characteristics for small arrays.

In this letter, we propose a method of substrate subtraction to examine the optimum shape of the substrate for improved antenna characteristics. The proposed method is applied to a three-element circular array, whose radiating elements are printed on a high-dielectric ceramic substrate. The shape of the substrate is then modified by subtracting three identical fan-shaped areas, and the shapes of the subtracted areas are varied by adjusting their radii and central angles. These parameters are important to avoid an undesired shift of the resonance frequency by maintaining the effective dielectric constant while reducing the dielectric loss caused by leakage fields between array elements. To demonstrate the improved properties, the array with the optimum shape of the substrate is fabricated, and its antenna characteristics are measured in a full anechoic chamber. We also performed parametric studies to observe variations of the directivity and the radiation efficiency in accordance with the design parameters of the fan-shaped areas. The results show that the proposed method of substrate subtraction is suitable for increasing the radiation gain in small circular arrays.

II. Proposed Method of Substrate Subtraction

A. Design Parameters

Fig. 1 shows the geometry of the three-element circular array and a 120-mm circular ground platform. The array has an array radius of r_2 and is composed of three identical elements. Each element has a circular patch having a radius of r_1 and is printed on a high-dielectric ceramic substrate ($\varepsilon_r = 20, \tan\delta = 0.0035$). Then, we subtract fan-shaped areas, where strong leakage fields are confined, from the ceramic substrate and vary their radius r_d and central angle θ_d to examine the optimum shape of the substrate. To achieve circular polarization (CP) properties, each radiating patch is connected to two ports with a phase difference of 90°, and the coordinates of Port 1 and Port 2 are adjusted by (X_1, Y_1) and (X_2, Y_2), respectively. The proposed structure is modeled as piecewise mesh triangles in FEKO EM Simulation Software from Altair Engineering Inc. [9], and detailed values of the design parameters are listed in Table I. The patch has a radius of approximately a quarter-wavelength, and the angle between Ports 1 and 2 with respect to the patch center is about 90° for impedance matching and CP characteristics. The optimum values of r_d and θ_d are 53.0 mm and 59°, respectively, which subtracts 38.3% from the substrate area.

Manuscript received November 23, 2016; accepted December 31, 2016. Date of publication January 16, 2017; date of current version June 12, 2017. This work was supported by the Civil Military Technology Cooperation and the Basic Science Research Program through the National Research Foundation of Korea funded by the Ministry of Education under Grant 2015R1A6A1A0303 1833.

T. Lee and H. Choo are with the School of Electronic and Electrical Engineering, Hongik University, Seoul 121-791, South Korea (e-mail: ltk4113@naver.com; hschoo@hongik.ac.kr).

D. Lee is with the Attached Institute of Electronics and Telecommunications Research Institute, Daejeon 34188, South Korea (e-mail: leedh@nsr.re.kr).

G. Byun is with the Research Institute of Science and Technology, Hongik University, Seoul 04066, South Korea (e-mail: kylebyun@gmail.com).

Color versions of one or more of the figures in this letter are available online at http://ieeexplore.ieee.org.

Digital Object Identifier 10.1109/LAWP.2017.2653191

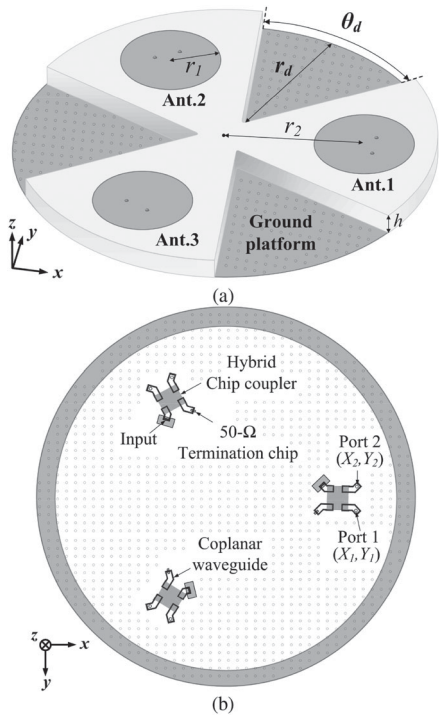

Fig. 1. Geometry of a three-element circular array with subtracted areas. (a) Perspective view of the array and its design parameters. (b) Layout of the PCB with a coupler circuit.

TABLE I
OPTIMIZED VALUES OF THE PROPOSED ARRAY

Parameters	Optimized values
r_1	14.1 mm
r_2	39.0 mm
r_d	53.0 mm
X_1	42.0 mm
X_2	45.6 mm
Y_1	2.7 mm
Y_2	−3.9 mm
θ_d	59.0°
h	6.0 mm

B. Measurement

To verify the feasibility of the substrate subtraction in terms of the improved radiation gain, the optimized shape of the ceramic substrate is fabricated, and the radiating elements are printed on top of the substrate by using the copper deposition mechanism with a thickness of 0.2 mm. We also fabricated a printed circuit board (PCB) with hybrid chip couplers (XC1400P−03S, Anaren), 50-Ω termination chips (MCR01 MZP F510, ROHM), and coplanar waveguides as transmission lines to achieve the 90°-phase difference between Ports 1 and 2, as shown in Fig. 2.

In our measurement process, Ant. 1 is actively fed, while Ant. 2 and Ant. 3 are terminated by 50-Ω loads. The reflection coefficients and bore-sight gain were measured in a semi-anechoic chamber using HP-8753D Network Analyzer from Hewlett Packard Inc. The active-element patterns and the axial ratio (AR) were measured in a full anechoic chamber

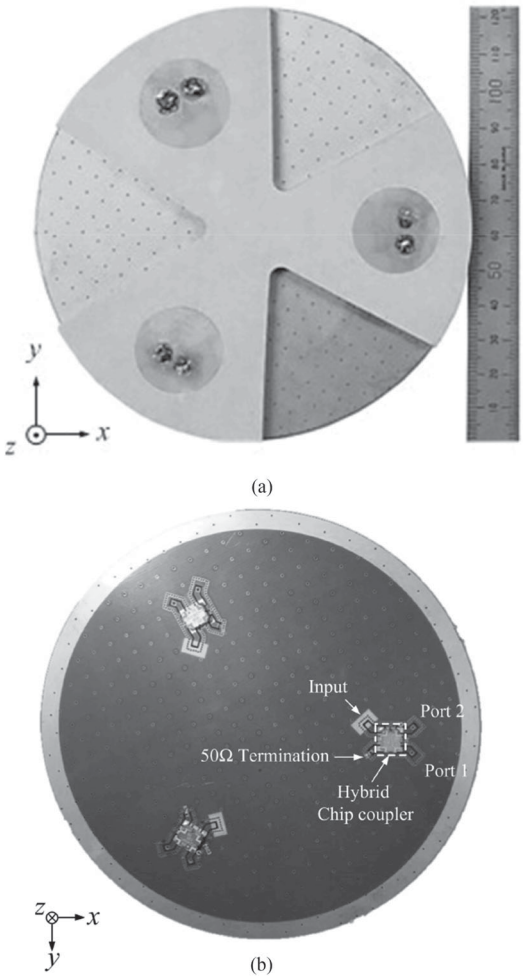

Fig. 2. Photographs of the fabricated array. (a) Top view with the printed radiating patches. (b) PCB embedding the coupler circuit.

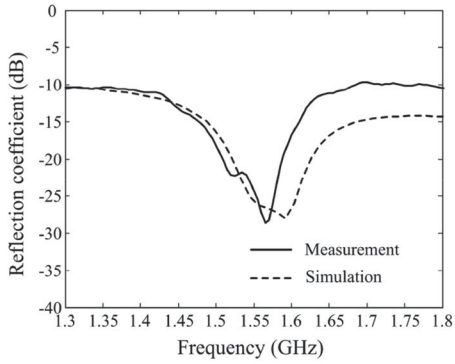

Fig. 3. Reflection coefficients of Ant. 1. Solid and dashed lines indicate measured and simulated results, respectively.

(15.2 × 7.9 × 7.9 m^3) using a quad-ridged horn antenna (Model: QRH-004060) at 11 frequency points using the E8362B Network Analyzer from Keysight Technologies Inc. Fig. 3 presents the measured and simulated reflection coefficients as a function of frequency. The circuit with the hybrid chip coupler, 50-Ω termination chip, and coplanar waveguides was built using Advanced Design System from Keysight Technologies Inc. [10], and the two-port scattering parameters of the

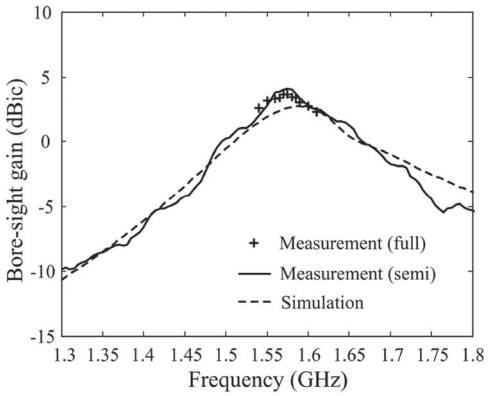

Fig. 4. Bore-sight gain of active-element patterns at Ant. 1. A dashed line indicates simulated results and is compared to the measured data obtained from semi and full anechoic chambers, which are specified by a solid line and "+" markers, respectively.

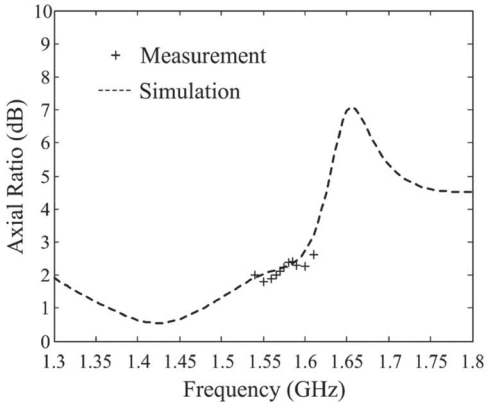

Fig. 5. Simulated axial ratio (AR) of Ant. 1 in comparison to measured data obtained from a full anechoic chamber.

antenna obtained from the FEKO EM simulator are imported as a two-port network to compute the simulated reflection coefficient in the input port. The dashed line indicates the simulated results, and the solid line represents the measured data. Both results show good agreement with the measured value of -26.2 dB at 1.575 GHz, which is similar to the simulated value of -26.9 dB.

Fig. 4 shows the measured and simulated right-hand circular gain values of the active-element patterns observed at the bore-sight direction. The simulated data are indicated by a dashed line, and the measured values obtained in the full and semianechoic chambers are specified by "+" markers and a solid line, respectively. The measured value of the full chamber is 3.6 dBic, and that of the semichamber is 3.9 dBic at 1.575 GHz, which is similar to the simulation having a peak value of 2.4 dBic.

Fig. 5 illustrates a comparison of the AR values in the bore-sight direction. The antenna has a broad CP bandwidth due to the use of the hybrid chip coupler and is circularly polarized with the measured AR value of 2.2 dB at 1.575 GHz.

Fig. 6(a) and (b) shows measured and simulated radiation patterns in the *zx*- and *zy*- planes at 1.575 GHz. The measured half-power beamwidths (HPBWs) are 115.6° in the *zx*- plane and 92.7° in the *zy*- plane, and simulated HPBWs are 118.4°

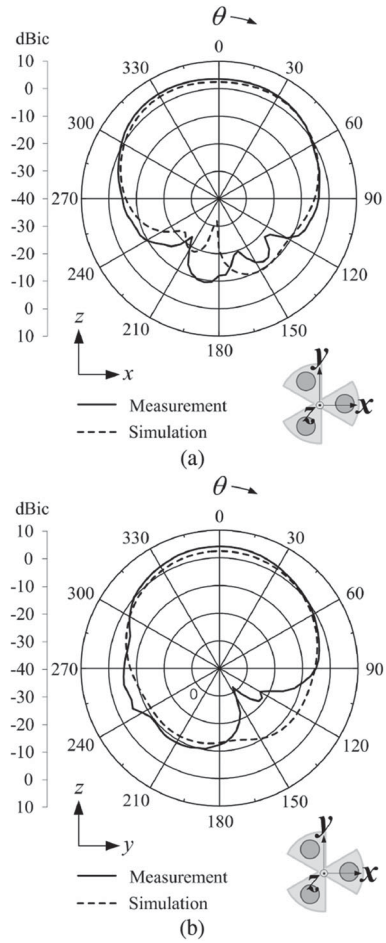

Fig. 6. Comparison of simulated and measured active element patterns at 1.575 GHz in (a) *zx*- and (b) *zy*- planes.

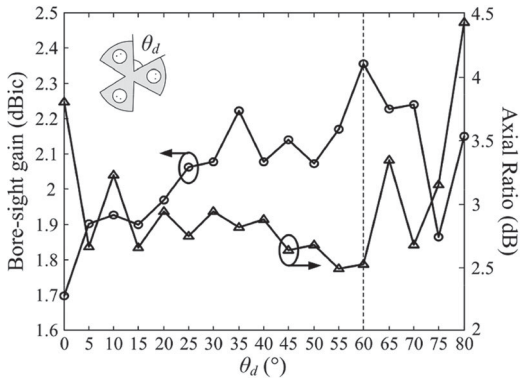

Fig. 7. Variations of the simulated bore-sight gain and the AR at 1.575 GHz according to θ_d at an interval of 5°, when $r_d = 53.0$ mm.

and 91.2° in the *zx*- and *zy*- planes, respectively. The patterns demonstrate that the substrate subtraction does not cause a pattern distortion in the upper hemisphere.

C. Analysis

Fig. 7 shows simulated results of the bore-sight gain and the AR according to the central angle θ_d of the fan-shaped area, when r_d is fixed to 53.0 mm. This subtraction area is varied by

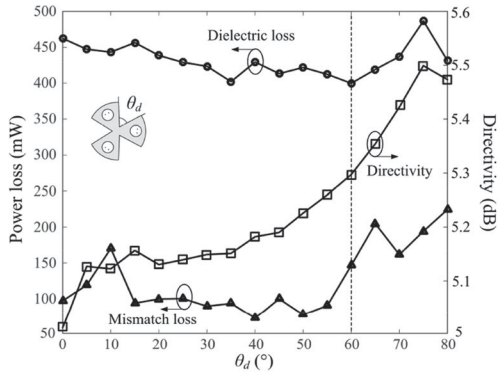

Fig. 8. Variations of power losses due to dielectric and impedance mismatch with the directivity for various θ_d ($r_d = 53.0$ mm). It is assumed that the conduction loss is neglected.

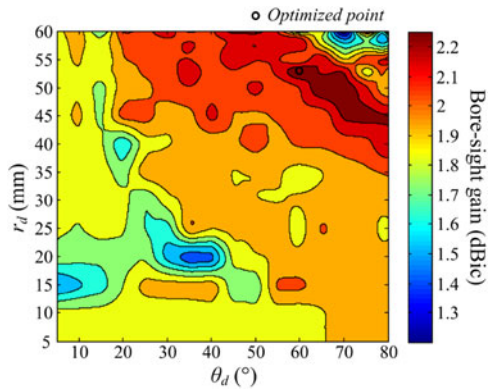

Fig. 9. Variations of the bore-sight gain obtained from active-element patterns according to the shape of fan-shaped areas that are determined by r_d and θ_d.

changing θ_d from 0° to 80°; e.g., the area can be adjusted from 0 mm^2 ($\theta_d = 0°$) to 5883 mm^2 ($\theta_d = 80°$). The bore-sight gain is increased to the maximum value of 2.4 dBic at $\theta_d = 60°$ and is decreased when θ_d is greater than 60°. The antenna maintains CP properties with the AR values of less than 3 dB from $\theta_d = 15°$ to $\theta_d = 60°$, and the AR is raised to 4.4 dB at $\theta_d = 80°$.

To interpret the reason for the improved bore-sight gain, we observe variations of power losses and directivity according to θ_d, as shown in Fig. 8. Both the dielectric and mismatch losses are calculated based on the assumption that the conducting materials of the antenna are the perfect electric conductor. The dielectric loss is decreased from 460 to 400 mW as θ_d becomes larger, while the mismatch loss is maintained below 160 mW. These results imply that the subtraction area is an important design factor to minimize the total effective loss tangent by reducing the leakage field strength between array elements. In addition, the substrate subtraction from $\theta_d = 15°$ to $\theta_d = 60°$ causes a very slight frequency shift of less than 50 MHz, and an undesired frequency shift occurs only when the subtracted area is placed in close proximity to the patch edges ($\theta_d \geq 70°$), which results in the mismatch loss of greater than 200 mW [11]. Thus, the peak radiation efficiency of 52% is observed at $\theta_d = 35°$ with a directivity of 5.1 dB. However, the realized gain value is greater at $\theta_d = 60°$ due to a higher directivity of 5.3 dB with a similar efficiency value of 51.8%, which is improved by 3.1% compared to the full substrate.

To generally observe the effectiveness of the substrate subtraction, we now observe variations of the bore-sight gain according to r_d and θ_d. r_d is varied from 5 to 60 mm at intervals of 5 mm, and θ_d is changed from 5° to 80° at intervals of 5°. The contours in Fig. 9 show that the bore-sight gain can be improved by increasing the area of the substrate subtraction, and the gain is drastically decreased when the area is too large ($\theta_d > 70°$ and $r_d > 55$ mm) because of the undesired frequency shift. Thus, we can verify that the substrate subtraction is capable of increasing the bore-sight gain by improving the directivity and the radiation efficiency.

III. Conclusion

We investigated the method of substrate subtraction to improve antenna characteristics in small arrays. The proposed method was applied to the three-element circular array to examine the optimum shape of the substrate, and three identical fan-shaped areas placed between the array elements were subtracted. We also performed parametric studies to interpret the reason for the gain improvement by observing variations in the directivity and the radiation efficiency. When the subtracted area is 38.3% compared to the entire substrate, the gain of the active-element pattern increases by 0.7 dB at the bore-sight direction, while the dielectric power dissipation decreases by 62.5 mW. The fabricated antenna showed that the bore-sight gain and the AR are 3.6 dBic and 2.2 dB, respectively. The results showed that the proposed method can improve the radiation gain by mitigating the unnecessary power losses.

References

[1] J. R. Lambert, C. A. Balanis, and D. DeCarlo, "Spherical cap adaptive antennas for GPS," *IEEE Trans. Antennas Propag.*, vol. 57, no. 2, pp. 406–413, Feb. 2009.

[2] G. Byun, H. Choo, and S. Kim, "Improvement of pattern null depth and width using a curved array with two subarrays for CRPA systems," *IEEE Trans. Antennas Propag.*, vol. 63, no. 6, pp. 2824–2827, Jun. 2015.

[3] G. Byun, S. M. Seo, I. Park, and H. Choo, "Design of small CRPA arrays for dual-band GPS Applications," *IEICE Trans. Commun.*, vol. E97-B, no. 6, pp. 1130–1138, Jun. 2014.

[4] G. Byun, J. Hyun, S. M. Seo, and H. Choo, "Optimum array configuration to improve null steering time for mobile CRPA systems," *J. Electromagn. Eng. Sci.*, vol. 16, no. 2, pp. 74–79, Apr. 2016.

[5] S. Weigand, G. H. Huff, K. H. Pan, and J. T. Bernhard, "Analysis and design of broad-band single-layer rectangular U-slot microstrip patch antennas," *IEEE Trans. Antennas Propag.*, vol. 51, no. 3, pp. 457–468, Mar. 2003.

[6] J. Anguera, E. Martnez-Ortigosa, C. Puente, C. Borja, and J. Soler, "Broadband triple-frequency microstrip patch radiator combining a dual-band modified Sierpinski fractal and a monoband antenna," *IEEE Trans. Antennas Propag.*, vol. 54, no. 11, pp. 3367–3373, Nov. 2006.

[7] K.-L. Wong and H.-C. Tung, "An inverted U-shaped patch antenna for compact operation," *IEEE Trans. Antennas Propag.*, vol. 51, no. 7, pp. 1647–1648, Jul. 2003.

[8] R. B. Waterhouse, "Improving the scan performance of probe-fed microstrip patch arrays on high dielectric constant substrates," *IEEE Trans. Antennas Propag.*, vol. 43, no. 7, pp. 705–712, Jul. 1995.

[9] FEKO EM Simulation Software, Altair Engineering Inc., 2015. [Online]. Available: http://www.altair.co.kr.

[10] Advanced Design System, Keysight Technologies Inc., 2013. [Online]. Available: http://www.keysight.com

[11] C. A. Balanis, "Microstrip antennas," in *Antenna Theory: Analysis and Design*, 3th ed. Hoboken, NJ, USA: Wiley, 2005, pp. 816–819.